Isotopic fingerprinting of biogeochemical processes and iron sources in the iron-limited surface Southern Ocean

Author(s):
Sieber, Matthias; Conway, Tim M.; De Souza, Gregory; Hassler, Christel S.; Ellwood, Michael J.; Vance, Derek

Publication date:
2021-08

Permanent link:
https://doi.org/10.3929/ethz-b-000485084

Originally published in:
Earth and Planetary Science Letters 567, https://doi.org/10.1016/j.epsl.2021.116967

Earth and Planetary Science Letters 567 (2021) 116967

Contents lists available at ScienceDirect

Earth and Planetary Science Letters

www.elsevier.com/locate/epsl

Isotopic fingerprinting of biogeochemical processes and iron sources in the iron-limited surface Southern Ocean

Sieber M.[a,*], Conway T.M.[b], de Souza G.F.[a], Hassler C.S.[c,d], Ellwood M.J.[e], Vance D.[a]

[a] Institute of Geochemistry and Petrology, Department of Earth Sciences, ETH Zurich, Zurich, Switzerland
[b] College of Marine Science and School of Geosciences, University of South Florida, FL, USA
[c] Department F.-A. Forel for Environmental and Aquatic Sciences, University of Geneva, Switzerland
[d] Swiss Polar Institute, EPF Lausanne, Lausanne, Switzerland
[e] Research School of Earth Sciences, Australian National University, Canberra, Australia

ARTICLE INFO

Article history:
Received 26 May 2020
Received in revised form 9 February 2021
Accepted 16 April 2021
Available online xxxx
Editor: Y. Asmerom

Keywords:
trace metals
micronutrients
biogeochemistry
nutrient cycling
Antarctic Circumnavigation Expedition

ABSTRACT

Iron (Fe) is an essential micronutrient that limits primary productivity throughout the surface of the Southern Ocean. Here, we present the first high-resolution depth profiles for dissolved Fe and Fe isotope ratios (δ^{56}Fe) from all major zones of the Southern Ocean, collected during the Antarctic Circumnavigation Expedition in austral summer 2017. Open-ocean surface waters are characterized by remarkably high δ^{56}Fe values (up to +1.6‰) and very low Fe concentrations (<0.05 nmol kg^{-1}). We attribute the elevated δ^{56}Fe values above the ferricline to the effect of continuous shallow cycling processes (uptake, recycling, and binding of Fe to organic ligands), with only a very limited resupply of Fe from below. Below the ferricline, δ^{56}Fe values approach ~0‰ and remain constant down to our deepest samples at 1000 m, with no obvious isotope signal from regeneration. This overall pattern in δ^{56}Fe is modified near islands, continental shelves and hydrothermal vents, where distinct δ^{56}Fe signatures are associated with different Fe sources. Near the volcanic Balleny Islands, elevated surface Fe concentrations associated with low δ^{56}Fe are indicative of reductive release of isotopically light Fe from sediments. Elevated δ^{56}Fe values at depth near the Balleny seamount chain and near the East Scotia Arc may reflect distal hydrothermal influences, caused by fractionation associated with precipitation or the loss of specific phases of Fe during long-range transport. Sedimentary sources of isotopically light Fe on the Antarctic Peninsula are important for shelf waters. Long-distance transport of this sediment-derived Fe and its influence on surface waters are strongly dependent on the regional circulation, and may ultimately be the source of light Fe previously observed within Antarctic Intermediate Water in the Atlantic sector of the Southern Ocean.

1. Introduction

The micronutrient iron (Fe) plays an essential role in photosynthesis and nitrogen fixation by marine microorganisms, with low dissolved Fe concentrations limiting primary production over large regions of the ocean (e.g. Morel et al., 2014). In the Southern Ocean, Fe limitation results from a deficiency in the supply of dissolved Fe relative to nitrate and phosphate from upwelling deep waters (e.g. Moore et al., 2002), a deficiency that is not sufficiently alleviated by external Fe sources (e.g. Boyd and Ellwood, 2010). Oceanic regions where macronutrients remain under-utilized are termed high-nutrient low-chlorophyll (HNLC). The largest of these HNLC regions, the Southern Ocean, plays a key role in global carbon cycling, mediating carbon transfer between the atmosphere and deep oceans (Gruber et al., 2019). Understanding the role of Fe in driving primary productivity and nutrient utilization in the Southern Ocean is vital for placing constraints on past, present and future global carbon cycling.

The Southern Ocean includes all waters south of the Subtropical Front (STF). Its dominant feature is the eastward Antarctic Circumpolar Current (ACC), which connects all three major ocean basins (Talley et al., 2011). Wind-driven upwelling within the ACC transports Upper Circumpolar Deep Water (UCDW) to the surface and this is the main source of macronutrients to the upper Southern Ocean. A portion of the upwelled waters flows southward, including into the gyres of the Ross and Weddell Seas. These two regions are important sites for the formation of the densest deep waters of the global ocean (Talley et al., 2011). Another portion of

* Corresponding author (present address): College of Marine Science, University of South Florida, FL, USA.
E-mail address: sieberm@usf.edu (M. Sieber).

https://doi.org/10.1016/j.epsl.2021.116967

the upwelling waters flows northwards as Antarctic Surface Water (AASW) and is eventually involved in the formation of the intermediate water masses Subantarctic Mode Water (SAMW) and Antarctic Intermediate Water (AAIW). Biological cycling in surface Southern Ocean waters results in the preferential partitioning of nutrients into different water masses, and the physical transport of these 'preformed signatures' is an important control on the global distribution of major nutrients (Sarmiento et al., 2004, 2007). Recently, the importance of the Southern Ocean in setting the global marine distribution of trace metals such as Cd and Zn and their isotopes has also been highlighted (e.g. Abouchami et al., 2014; Vance et al., 2017; Sieber et al., 2019a).

Despite recent advances in our understanding of Southern Ocean metal cycling and an intense interest in Fe, the controls on the distribution of Fe in the Southern Ocean remain poorly understood, largely due to the difficulty of measuring Fe at such low dissolved concentrations (<0.1 nmol kg^{-1}). Dissolved Fe is mainly supplied to the surface ocean by upwelling and deep winter mixing, utilized by primary production during spring and sustained by shallow Fe recycling during summer (Bowie et al., 2001; Tagliabue et al., 2014). Due to the relatively low supply of dissolved Fe by the otherwise nutrient-rich upwelling waters, Fe limitation of phytoplankton occurs over large regions of the surface Southern Ocean (Moore et al., 2013). Since dust inputs are considerably lower in the Southern Ocean than in most other regions of the global ocean (Hamilton et al., 2019), localized Fe inputs from other external sources are important. The most prominent Fe sources identified to date include sedimentary Fe release on the Antarctic shelf and/or near Southern Ocean islands (e.g. Planquette et al., 2011; Sherrell et al., 2018) and hydrothermal venting (Resing et al., 2015; Klar et al., 2017; Ardyna et al., 2019). The influence of sedimentary Fe sources from the Antarctic Peninsula can be traced over long distances along the shelf and into the waters of the Weddell Gyre (e.g. de Jong et al., 2012; Hatta et al., 2013; Measures et al., 2013; Klunder et al., 2014). Furthermore, Fe is supplied to nearshore waters via meltwater inputs from Antarctic ice shelves (e.g. Arrigo et al., 2015; Gerringa et al., 2015) and the melting of icebergs, floating ice shelves and sea ice (e.g. Lannuzel et al., 2016).

In the last decade, Fe stable isotope ratios (δ^{56}Fe) have begun to provide constraints on various processes that are part of the Fe cycle. Iron isotopes have been shown to fingerprint and trace key Fe sources through ocean basins (Radic et al., 2011; Conway and John, 2014). Iron can be released from sediments via two pathways: Fe(III) reduction during respiration of organic matter, or non-reductive sediment dissolution (Radic et al., 2011; Homoky et al., 2013). The δ^{56}Fe of both endmembers is reasonably well constrained by porewater measurements, with Fe released by reductive dissolution significantly lighter (down to -3‰) than Fe released during non-reductive dissolution ($+0.1$‰; Homoky et al., 2013). By contrast, although hydrothermal vent fluid δ^{56}Fe signatures occupy a fairly narrow range (-0.7 to -0.1‰; as summarized in Lough et al., 2017), proximal and distal hydrothermal signals in the water column span a large range (-1 to $+2$‰) due to modification of the source signal by oxidation and precipitation reactions, as well as scavenging and ligand-binding processes (Severmann et al., 2004; Conway and John, 2014; Ellwood et al., 2015; Fitzsimmons et al., 2017; Klar et al., 2017). This large range in potential distal hydrothermal δ^{56}Fe signatures means that further process studies providing vent-specific and regional information are required in order for δ^{56}Fe to be a diagnostic hydrothermal tracer at the basin scale. Finally, natural atmospheric dust is known to have a crustal δ^{56}Fe signature ($+0.1$‰; Beard et al., 2003), but the net δ^{56}Fe signature of dissolved Fe released upon dissolution has been hypothesized to be heavy (Conway and John, 2014), due to the binding of heavy Fe by organic ligands in the dissolved phase (Dideriksen et al., 2008; Morgan et al., 2010).

Dissolved δ^{56}Fe can also provide insight into a range of processes, such as biological uptake, scavenging, regeneration, ligand-binding, and transformation of redox species, which occur both within the water column and at oceanic interfaces (e.g. Ilina et al., 2013; Ellwood et al., 2015, 2020; Fitzsimmons et al., 2015, 2017). While culturing constraints on fractionation of Fe isotopes during biological uptake remain absent, field studies have pointed to the importance of this process in driving surface waters to high δ^{56}Fe values, especially during bloom events (Ellwood et al., 2015, 2020). Additionally, elevated δ^{56}Fe in the soluble size fraction (<0.02 µm; Fitzsimmons et al., 2015), and during lab experiments with Fe(III)-binding siderophores, have been attributed to preferential ligand binding to heavier Fe isotopes (Dideriksen et al., 2008; Morgan et al., 2010). Some studies have attributed isotopically light Fe at depth to regeneration (Radic et al., 2011; Abadie et al., 2017), though this does not appear to be a widespread pattern in GEOTRACES datasets (Schlitzer et al., 2018). Overall, the effects of scavenging, biological uptake and regeneration on oceanic δ^{56}Fe distributions remain poorly understood, due to a paucity of available field and culture data.

Although many studies have focused on the distribution of dissolved Fe in the Southern Ocean, dissolved δ^{56}Fe data remain extremely sparse, with only a handful of water column profiles available (Fig. 1; Abadie et al., 2017; Ellwood et al., 2020). Here, we present 17 profiles of high-depth-resolution dissolved Fe concentration and δ^{56}Fe from the upper 1000 m of the water column in the Pacific and Atlantic sectors of the Southern Ocean, covering all the major Southern Ocean zones. These include locations close to the Balleny Islands, inside the Mertz Glacier Polynya, near the Antarctic Peninsula and west of the Drake Passage (Fig. 1). The high shallow-subsurface resolution of our dataset allows us to investigate the effects of surface and near-surface processes on δ^{56}Fe, as well as the local and regional influence of sources on the distribution of Fe and its isotopes in the Southern Ocean. Our data also allow us to examine the suggestion that Southern Ocean processes create 'preformed' δ^{56}Fe signatures that reach the Southern Atlantic Ocean (Abadie et al., 2017).

2. Oceanographic setting

Samples discussed here were collected from the Atlantic and Pacific sectors of the Southern Ocean, in all major Southern Ocean zones. These zones (Southern, Antarctic, Polar Frontal and Subantarctic as defined by Talley et al. (2011)) are separated from each other by the major dynamic and biogeochemical fronts of the Southern Ocean (Fig. 1). Closest to the continental shelf, and encompassing the Ross and Weddell Gyres, is the Southern Zone (SZ). This zone is bounded to the north by the Southern Boundary (SB), which is marked by the most southerly outcropping of UCDW (Orsi et al., 1995). The other zones are subdivided by the three major fronts of the ACC, namely the most-northerly Subantarctic Front (SAF), the central Antarctic Polar Front (APF) and the most-southerly Southern ACC Front (SACCF). In the Antarctic Zone (AZ), between the SACCF and the APF, wind-driven upwelling brings nutrient-rich UCDW to the surface (Talley et al., 2011). Ekman transport carries Antarctic Surface Water (AASW) northwards, across the APF and into the Polar Frontal Zone (PFZ). To the north, the Subantarctic Zone (SAZ) is separated from the Polar Frontal Zone by the SAF. It is here, in the PFZ and SAZ, that the intermediate water masses SAMW and AAIW form (Sallée et al., 2010), before crossing the subtropical front (STF) and leaving the Southern Ocean.

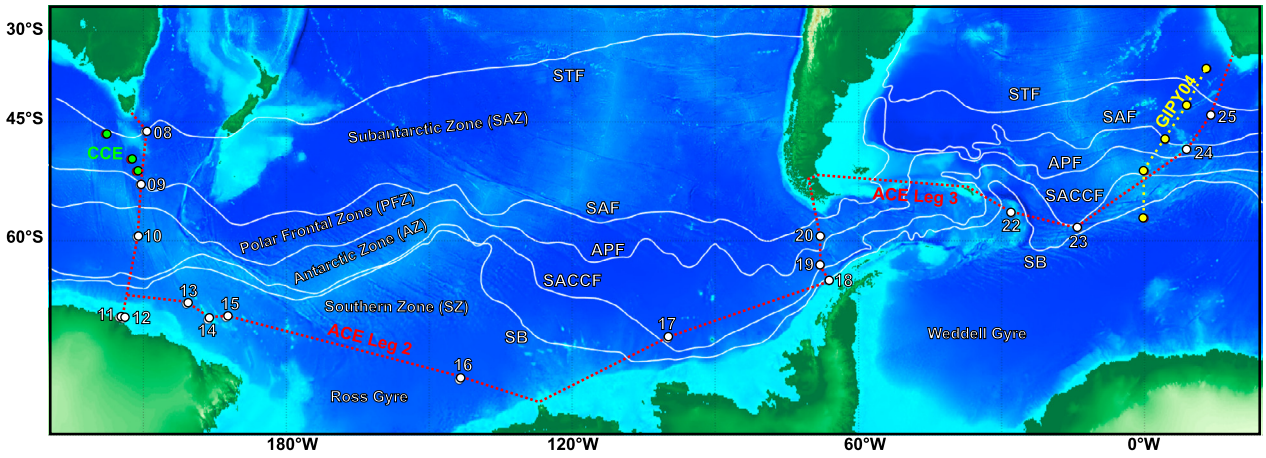

Fig. 1. Bathymetric map of the Pacific and Atlantic sectors of the Southern Ocean showing the location of stations sampled during Legs 2 and 3 of the Antarctic Circumnavigation Expedition (red line). The station locations where water column profiles of δ^{56}Fe have been measured previously in the Southern Ocean are shown in green (cold core eddy (CCE); Ellwood et al., 2020) and yellow (GIPY04; Abadie et al., 2017). Southern Ocean front locations follow Orsi et al. (1995) and are represented by white lines: Subtropical Front (STF), Subantarctic Front (SAF), Antarctic Polar Front (APF), Southern ACC Front (SACCF), and Southern Boundary (SB). (For interpretation of the colors in the figure(s), the reader is referred to the web version of this article.)

3. Methods

Seawater samples were collected during the Antarctic Circumnavigation Expedition (Legs 2, 3) onboard the R/V Akademik Tryoshnikov during austral summer 2017 (January - March 2017). Depth profiles spanning the uppermost 1000 m of the water column, with particular focus on high depth-resolution in the top 200 m (6–8 samples), were sampled for dissolved Fe and δ^{56}Fe at seventeen stations (ACE station numbers 08–20, 22–25) in the Atlantic and Pacific sectors of the Southern Ocean (Fig. 1).

The sample collection method for filtered seawater samples (volumes of 1 L or 4 L) was previously reported in Sieber et al. (2019a). Trace metal extraction was carried out at ETH Zürich following a previously published method (Sieber et al., 2019a). Briefly, a ^{57}Fe–^{58}Fe double spike was added (sample-to-spike ratio of 1:2) prior to batch extraction of metals from seawater using Nobias PA-1 chelating resin (Conway et al., 2013). Metals were eluted from the resin and purified by an anion-exchange chromatography technique using 20 µL PTFE micro-columns filled with AG-MP1 resin, as described in Sieber et al. (2019a). The Fe fraction was eluted with 1 M HCl, then evaporated to dryness and redissolved in 0.3 M HNO_3 for analysis by MC-ICPMS. The same method was used for 1 L and 4 L samples and has a total procedural blank of ~0.4 ng (n = 5) per liter of seawater. It has been shown previously to effectively purify Fe from major cations and interfering elements (Conway et al., 2013).

Fe isotope analyses were performed on a Thermo Neptune Plus Multi-Collector-ICPMS in the Tampa Bay Plasma Facility at the University of South Florida. Samples were introduced using a PFA nebulizer with a flow rate of ~120 µl/min, an Apex Ω membrane desolvating system (Elemental Scientific), and Ni Jet sampler and Al X-type skimmer cones. Instrumental mass bias was corrected for using the double spike technique, with data reduction following Siebert et al. (2001). Beam sizes of ^{52}Cr and ^{60}Ni were measured simultaneously and used to correct isobaric interferences on ^{54}Fe and ^{58}Fe, respectively. Iron stable isotope ratios are expressed relative to the mean of a pair of mixtures of the isotopic standard IRMM-014 and our double spike, which were analyzed before and after each block of five samples. Iron isotope ratios are expressed in standard delta notation:

$$\delta^{56/54}Fe = \left[\frac{(^{56}Fe/^{54}Fe)_{sample}}{(^{56}Fe/^{54}Fe)_{IRMM-014}} - 1 \right] \times 1000$$

While this method is well established and has been intercompared for the range of open ocean seawater Fe concentrations typically encountered (0.1 – 1 nmol kg^{-1}), concentrations in samples in this study reached as low as 0.01 nmol kg^{-1}, equivalent to 0.55 ng in 1 L and 2.2 ng in 4 L seawater samples, respectively. To ensure that δ^{56}Fe was being measured accurately at such low analyte amounts, a suite of IRMM-014–double spike mixtures were analyzed during each analytical session. This procedure showed that IRRM-014 could be measured accurately (reproducible δ^{56}Fe within 2SE of 0‰) down to a sample size of 5 ng, which is comparable to previous studies (~6 ng; Conway and John, 2014). We thus regard this as the lower limit for the method used here, and do not report dissolved δ^{56}Fe for samples that contain less than 5 ng of dissolved Fe, i.e. with Fe concentrations of 0.09 nmol kg^{-1} in 1 L and 0.022 nmol kg^{-1} in 4 L seawater samples.

Because of the lack of large-volume seawater samples for multiple extraction and analysis, long-term instrumental precision was assessed through repeat measurements of a secondary Fe standard solution (NIST-3126) for which we obtain a δ^{56}Fe value of +0.36 ± 0.04‰ (2SD, n = 351 during 24 sessions over 3 years). We apply this value as an estimate of 2σ uncertainty on δ^{56}Fe for all samples, except for low concentration samples where the larger internal error is a more conservative estimate of uncertainty. Concentrations reported herein were calculated using the isotope dilution technique based on the ^{57}Fe/^{56}Fe ratios from the isotope analyses. We assign a 2% uncertainty to concentrations measured using this approach (Conway et al., 2013). The accuracy of this technique for both Fe concentrations and δ^{56}Fe has been demonstrated previously on SAFe seawater samples and through intercalibration with other groups (Conway et al., 2013; Ellwood et al., 2020). We report one new measurement of Fe in SAFE D2 (0.95 nmol kg^{-1}, δ^{56}Fe of −0.20 ± 0.09, 2SE) which was processed alongside the samples measured here using the same double spike solution and measured on a Neptune Plus MC-ICPMS at ETH Zurich. This result agrees with both consensus concentrations and previously reported δ^{56}Fe values (Conway et al., 2013). Our Atlantic sector data are compared with those of Abadie et al. (2017) in Supplementary Fig S1.

4. Results and discussion

Dissolved Fe and δ^{56}Fe from all zones of the Southern Ocean are tabulated in Supplementary Data and presented in Figs. 2 and 5–7. We discuss these results in the context of the processes affecting the distribution of Fe and its isotopes, and thus present the

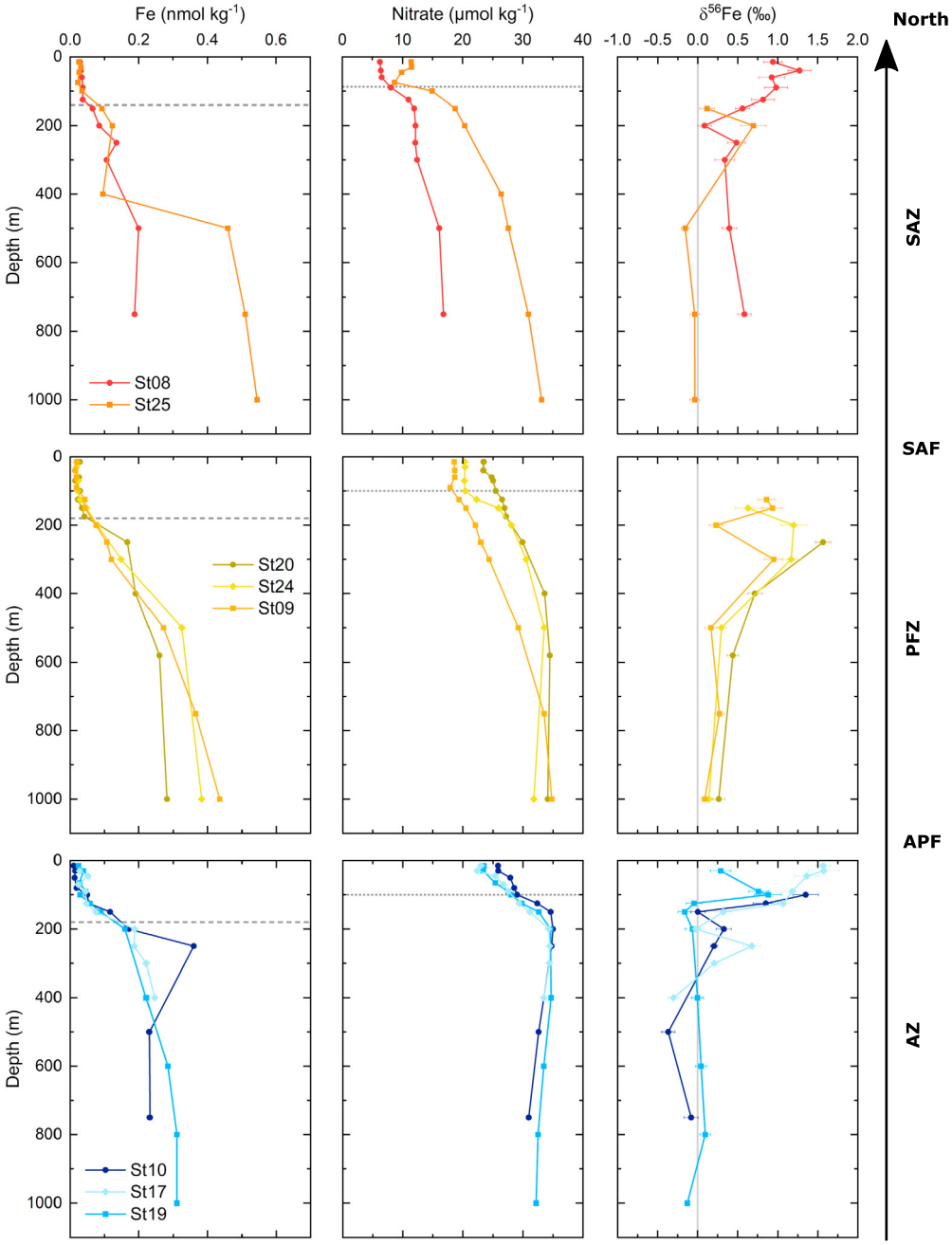

Fig. 2. Depth profiles of dissolved Fe, nitrate and δ^{56}Fe across the major Southern Ocean zones, Subantarctic Zone (SAZ), Polar Frontal Zone (PFZ), Antarctic Zone (AZ) separated by the Subantarctic Front (SAF) and Antarctic Polar Front (APF); see Fig. 1. Depths of the ferriclines and nitraclines are indicated by the dashed and dotted lines, respectively.

first effort to characterize Fe isotope systematics in the upper waters of the Southern Ocean. First, we discuss how biological uptake and regeneration, complexation, seasonal mixing and upwelling of deep waters influence the distribution of Fe and δ^{56}Fe in surface waters. Second, we explore the influence of local continental, island and hydrothermal Fe sources on the local and regional distribution of Fe and δ^{56}Fe. Finally, we reconsider the role of large-scale ocean circulation in influencing δ^{56}Fe signatures of waters north of the APF and in the lower-latitude Atlantic Ocean.

4.1. The role of surface processes in setting δ^{56}Fe

Open-ocean surface waters (above 100 m) are extremely depleted in dissolved Fe (as low as 0.01 nmol kg^{-1}), and Fe concentrations remain below 0.05 nmol kg^{-1} across all biogeochemical zones of the Southern Ocean (Fig. 2). These low concentrations are the result of the near-complete summer uptake of Fe by phytoplankton, due to a deficiency in its supply from upwelling deep waters relative to nitrate and phosphate. However, despite the strong drawdown of Fe at the surface, dissolved Fe concentration profiles do not show a clear complementary regeneration signal in the shallow subsurface (<100 m; Fig. 2), as do nitrate or other trace metals like Cd (e.g. Sieber et al., 2019a). Iron released via shallow regeneration is either quickly taken up again by phytoplankton (rapid recycling) or scavenged onto abiotic particles (Bowie et al., 2001), and therefore is not obviously identifiable in the dissolved pool. This is in good agreement with recent findings from a Southern Ocean cold-core eddy (Ellwood et al., 2020), sug-

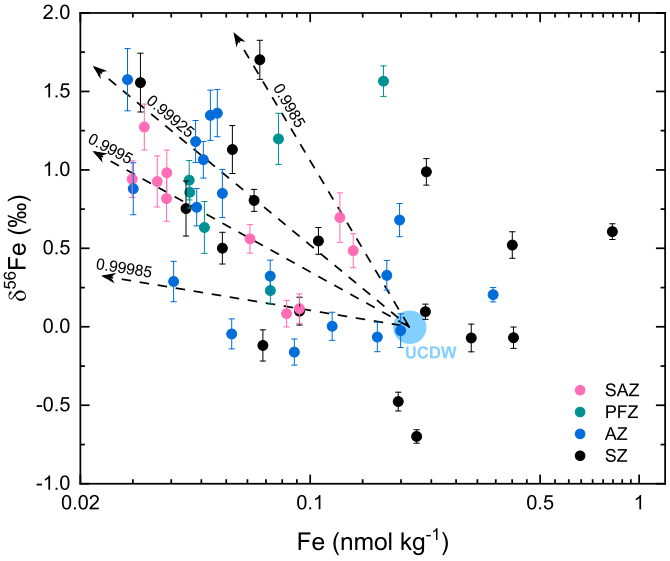

Fig. 3. Iron isotope systematics in the top 300 m of all open ocean stations, color-coded for the Southern Ocean zones: Subantarctic Zone (SAZ), Polar Frontal Zone (PFZ), Antarctic Zone (AZ) and Southern Zone (SZ). As a visual reference, dashed lines represent Rayleigh fractionation trends with different fractionation factors α, where $\alpha = R_{phytoplankton}/R_{seawater}$ and $R = {}^{56}Fe/{}^{54}Fe$, and using the signature of upwelled UCDW to as the starting composition of any fractionation in the surface ocean.

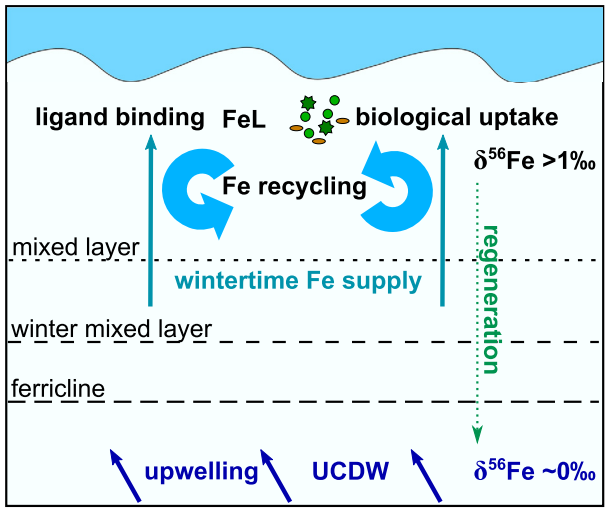

Fig. 4. Schematic representation of the dominant processes controlling the distribution of Fe isotopes in the surface Southern Ocean, after Tagliabue et al. (2014).

gesting that Fe has a very short residence time in surface waters across the Southern Ocean, being rapidly recycled between the dissolved pool and phytoplankton.

Below the low-Fe surface waters, Fe concentrations exhibit a pronounced increase at 100 – 300 m (to 0.10 – 0.36 nmol kg^{-1}; Fig. 2), driven by the release of Fe from sinking particles and, south of the APF, upwelling of comparatively Fe-rich UCDW (~250 m). The depth at which the vertical concentration gradient (∂Fe/∂z) is at a maximum, termed the ferricline, is around 150 – 200 m, deeper than the nitracline and the base of the winter mixed layer (WML), both occurring at ~100 m (Fig. 2; see also Janssen et al., 2020). While the depth of the ferricline in our dataset shows relatively little variation across the Southern Ocean zones, the vertical Fe gradient at the ferricline does decrease from south to north, meaning that the ferricline is sharper further south (Fig. 2). This is due to a change in the processes that dominantly drive the Fe increase: north of the APF, the Fe increase is driven by deep mixing and gradual Fe release from particles, while south of the APF it is the upwelling of UCDW that is important. Deeper waters (below 300 m) at all open ocean stations exhibit a slight increase in Fe over the depth range of the profiles, likely the result of gradual release of dissolved Fe from sinking particles.

The extremely low dissolved Fe concentrations (<0.05 nmol kg^{-1}) in surface waters are associated with remarkably high dissolved δ^{56}Fe (> + 1‰; Fig. 2) across all Southern Ocean zones, which is similar to recent observations from a Southern Ocean eddy (Ellwood et al., 2020). That study suggested that isotopically heavy surface Fe could be explained either by a preference for isotopically light Fe during biological uptake, or by a combination of uptake, regeneration, scavenging and complexation by organic ligands (Ellwood et al., 2020). While culture data has not yet provided insight into the fractionation effect of biological uptake mechanisms, complexation by organic ligands is known to preferentially bind heavy Fe (Dideriksen et al., 2008; Morgan et al., 2010). The fact that our Southern Ocean data do not follow simple Rayleigh systematics (Fig. 3), supports the suggestion that, unlike elements such as Cd (e.g. Abouchami et al., 2014), the isotopically heavy Fe is not controlled by a single isotope fractionation process. Instead, the scatter suggests that biological uptake, rapid recycling, and complexation to organic ligands all play a role in driving surface δ^{56}Fe to high values. Overall, these surface processes, together with a deep ferricline and a limited supply of Fe from below, result in a surface cycling loop that keeps dissolved Fe concentrations low and drives δ^{56}Fe in surface waters to higher and higher values (similar to that proposed by Rafter et al. (2017) and Tagliabue et al. (2014) for surface regions with low external Fe supply; Fig. 4).

South of the APF, as Fe concentrations increase through the ferricline, δ^{56}Fe decreases from high values at the surface to ~0‰ around 200 −300 m depth, and generally remains fairly constant below (Fig. 2). This change is mainly driven by the presence of upwelling UCDW at depth (~0.2 nmol kg^{-1}, ~0‰; Fig. 2). Further north, in the PFZ and SAZ, the elevated surface δ^{56}Fe signal extends to greater depths, and a more gradual return towards ~0‰ reflects deeper mixing in these zones (Fig. 2).

4.2. Regional Fe sources

4.2.1. Margin sediments (Mertz Glacier Polynya and Antarctic Peninsula)

Surface seawater samples collected within the Mertz Polynya on the Antarctic Shelf near Mertz Glacier (Fig. 1; Stations 11, 12) exhibit anomalously low macronutrient and trace metal concentrations compared to other stations south of the SB (Sieber et al., 2019b, 2020; Janssen et al., 2020). Those studies showed that there is meltwater input to surface waters, but the associated dilution effect is insufficient to explain the low surface concentrations. Rather, they suggested that low surface concentrations are the result of increased biological activity due to a local supply of dissolved and/or particulate Fe (Sieber et al., 2019b, 2020; Janssen et al., 2020). The fact that these stations show similarly low surface Fe concentrations as open ocean waters (<0.05 nmol kg^{-1}; Fig. 5a) suggests that any Fe reaching surface waters is quickly utilized by phytoplankton. Furthermore, surface waters exhibit similar δ^{56}Fe values to the open ocean waters (+0.4 to +1.2‰; Fig. 5a). However, unlike the open ocean dataset, the data from the upper ~200 m of the Mertz Polynya do follow a clear Rayleigh fractionation trend (Fig. 5b). A strong seasonal phytoplankton bloom after the opening of the polynya would drive high-uptake high-export dynamics that are most similar to a unidirectional process, and thus most likely to produce a Rayleigh trend within the surface and shallow subsurface. Therefore, this Rayleigh trend

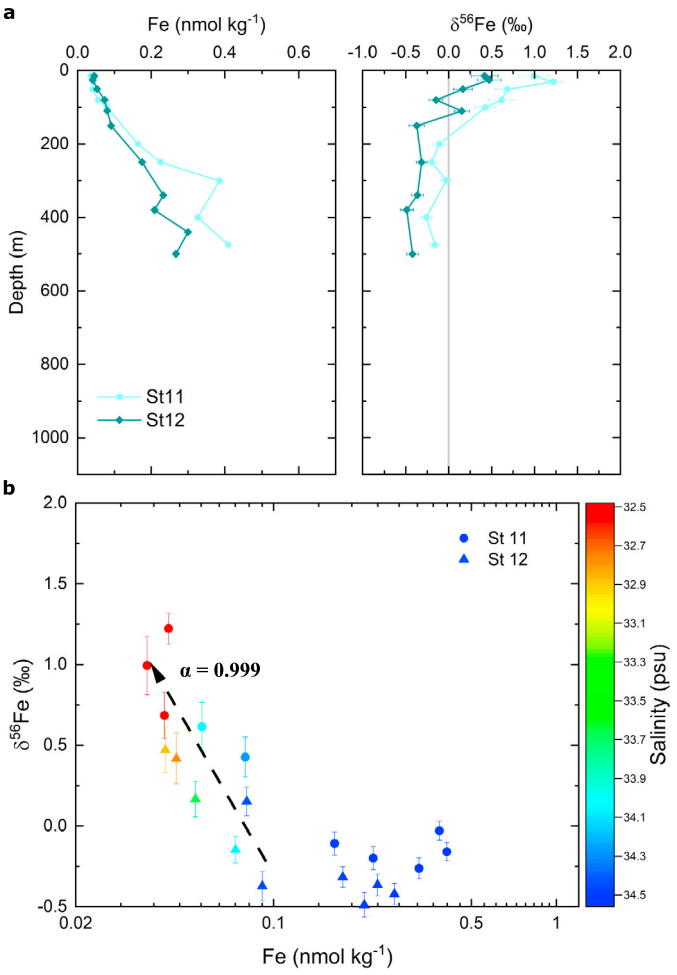

Fig. 5. Iron isotopes in the region of the Mertz Glacier. (a) Depth profiles of dissolved Fe and δ^{56}Fe of Stations 11 and 12 located in the Mertz Glacier Polynya. (b) Fe isotope systematics for the same stations, colored for salinity. Surface waters follow a Rayleigh fractionation trend (black arrow) driven by biological uptake with a fractionation factor α of 0.999 (based on regression using data from the top 200 m), similar to observations in a cold core eddy (α = 0.999; Ellwood et al., 2020), where $\alpha = R_{phytoplankton}/R_{seawater}$ and $R = {}^{56}Fe/{}^{54}Fe$.

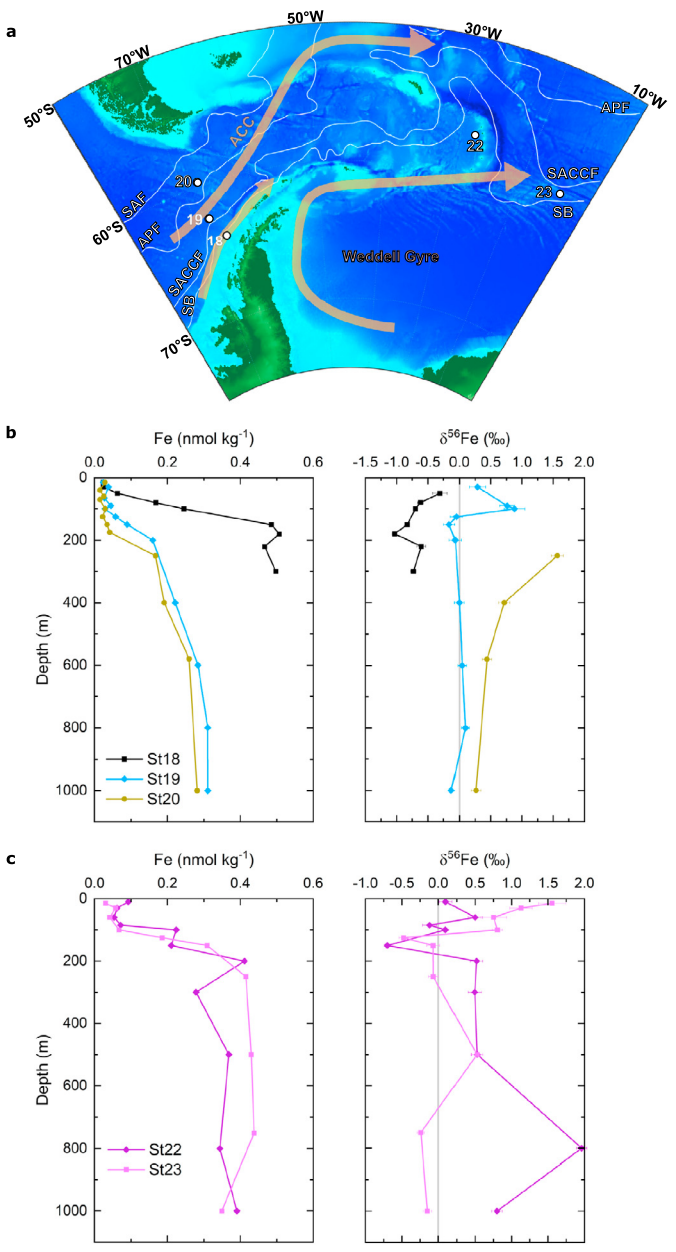

Fig. 6. (a) Map showing stations near the Antarctic Peninsula with the arrows indicating the main circulation features in the area: Antarctic Circumpolar Current (ACC) and the Weddell Gyre. (b) Depth profiles of dissolved Fe and δ^{56}Fe of stations located near the Drake Passage on the Antarctic shelf (18), in the AZ (19) and the PFZ (20). (c) Depth profiles of dissolved Fe and δ^{56}Fe of stations located in the Weddell Gyre (22, 23).

may indicate that the surface δ^{56}Fe inside the polynya is more strongly dominated by a single process such as biological uptake ($\alpha = 0.999$), as has been suggested within isolated Southern Ocean eddies ($\alpha = 0.999$; Ellwood et al., 2020).

Below the surface, Fe concentrations show a near-linear increase down to 500 m, reaching up to ~0.4 nmol kg^{-1} (Fig. 5a). Dissolved δ^{56}Fe gradually transition to lower values with depth in the upper 150 – 200 m (to δ^{56}Fe = –0.11‰ at Station 11 and –0.37‰ at Station 12) and remain relatively invariant below this, despite an increase in Fe concentration (Fig. 5a). Isotopically light Fe associated with elevated concentration at depth indicates a sediment source to the water column, consistent with previous observations on the continental shelf (e.g. Ardelan et al., 2010; Sherrell et al., 2018). The near-constant offset in δ^{56}Fe profiles between Stations 11 and 12 may reflect subtle differences in the type of sedimentary Fe sources to the water column. For example, reductive dissolution may be more important at Station 12, leading to lighter δ^{56}Fe, while more Fe could be supplied via non-reductive dissolution of sediments at Station 11, resulting in more near-crustal dissolved δ^{56}Fe values (~−0.15‰).

An offshore transect from the West Antarctic Peninsula also provides an opportunity to assess the influence of continental Fe fluxes on open-ocean waters. We observe a pronounced subsurface signal of elevated Fe concentrations and low δ^{56}Fe at Station 18 on the continental shelf near the Antarctic Peninsula (Fig. 6a). While surface waters show similarly low Fe concentrations to open-ocean waters (down to 0.02 nmol kg^{-1}), there is a steep increase to ~0.5 nmol kg^{-1} at 150 m, hence a shallow and extremely strong ferricline, and near-constant Fe concentrations below (Fig. 6b). This concentration gradient is associated with a δ^{56}Fe transition from −0.3‰ near the surface to a minimum of −1‰ at 180 m, with δ^{56}Fe decreasing as Fe concentrations increase in the subsurface (Fig. 6b). The low δ^{56}Fe throughout the water column suggests that sedimentary release of Fe via reductive dissolution is the primary source of Fe, even to surface waters. A dominant sedimentary source would be consistent with recent studies (e.g. Sherrell et al., 2018), although an input of isotopically light Fe via subglacial discharge could also contribute to such a signal (Henkel et al., 2018).

An increase in δ^{56}Fe towards the surface indicates that biological activity also influences surface δ^{56}Fe signatures here, although surface δ^{56}Fe values never exceed 0‰.

Previous studies have proposed that Fe from such sedimentary sources along the Antarctic Peninsula may be transported over long distances, and might affect the low-Fe open-ocean waters of the Drake Passage and/or the Weddell Gyre (de Jong et al., 2012; Hatta et al., 2013; Klunder et al., 2014). Our dataset for the upper Southern Ocean allows us to investigate whether sedimentary sources on the Antarctic Peninsula affect upper ocean waters to the north, near the Drake Passage (Stations 19, 20) and to the east, in the Weddell Gyre (Stations 22, 23). Fig. 6b shows that there is no obvious transport of light Fe from the Antarctic Peninsula into the ACC near the Drake Passage, likely due to the northeastward flow of the circulation along the outer shelf (Fig. 6a); rather, Stations 19 and 20 show the same features as other stations in the AZ and PFZ (Fig. 2). The fact that the strong near-zonal circulation along the Antarctic Peninsula prevents shelf-derived Fe from extending northward into open waters west of the Drake Passage is of relevance to the global and basinal scale Fe distribution, since this area is the main formation region of AAIW (Sallée et al., 2010; see section 4.3).

However, there is evidence in our dataset to support previous studies suggesting that Fe originating from sedimentary sources along the Antarctic Peninsula and nearby islands is transported in shallow waters over long distances into the Weddell Gyre (e.g. Hatta et al., 2013; Measures et al., 2013; Jiang et al., 2019). Stations 22 and 23 in the Weddell Gyre exhibit elevated Fe concentrations and distinctly low δ^{56}Fe at depths of 100 – 150 m (Fig. 6c), consistent with previous observations in the Weddell Gyre (Abadie et al., 2017; Fig. S1). We propose that these light Fe signatures ultimately originate from sedimentary sources along the Antarctic Peninsula or the islands east of it. With increasing distance from the source region, Fe is removed from the shallow surface system by the processes described in Section 4.1, overprinting the source δ^{56}Fe signal and driving surface δ^{56}Fe to higher values (Fig. 6c). However, the low-δ^{56}Fe signal is preserved below the WML as far west as Station 23, suggesting that sedimentary sources near the Antarctic Peninsula have an influence on large parts of the Weddell Gyre.

4.2.2. Sediments around the Balleny Islands

Stations 13 and 14, located in the vicinity of the volcanic Balleny Islands, show slightly elevated surface Fe concentrations (up to 0.08 nmol kg^{-1}) followed by a sharp increase down to the base of the WML (up to 0.34 nmol kg^{-1} at ~100 m; Fig. 7a). Consequently, these stations exhibit a much shallower and sharper ferricline than open ocean stations (Fig. 2). These high Fe concentrations, which occur within the WML, are strongly indicative of Fe supply from the Balleny Islands, resulting in natural Fe fertilization of surface waters analogous to that observed at other Antarctic island chains (e.g. Planquette et al., 2011). This is consistent with satellite observations of elevated chlorophyll-*a* concentrations indicating elevated productivity at the time of sampling (Fig. 7b).

Near the Balleny Islands, at Station 14, elevated Fe concentrations in surface waters and the WML are associated with low δ^{56}Fe values (−0.28‰, n=2 in the top 30 m; −0.68‰ at 100 m in the WML). This is consistent with Fe supply to shallow waters from the reductive release of isotopically light Fe from sediments around the Balleny Islands, with the WML likely reflecting the source signature. With distance from the islands, surface Fe concentrations decrease, and δ^{56}Fe returns to elevated values (+0.75‰, n=2 in the top 30 m at Station 13; Fig. 7a). This indicates a transition to the surface δ^{56}Fe cycling regime observed elsewhere under Fe limitation (see Section 4.1); nonetheless, the influence of the local Fe source continues to be reflected in the WML that exhibits negative

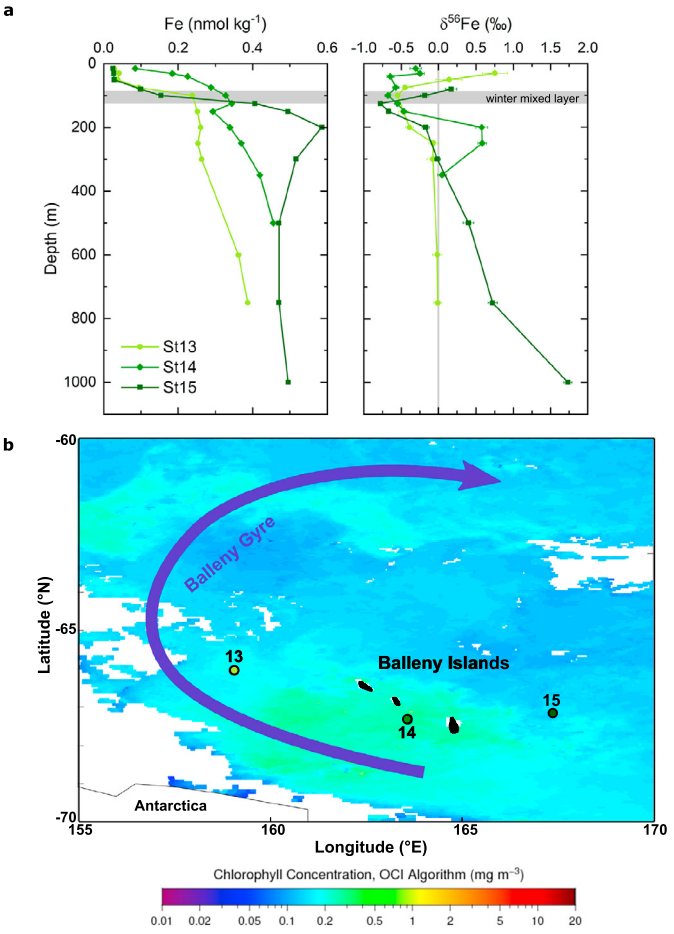

Fig. 7. (a) Dissolved Fe concentration and Fe isotope depth profiles near the Balleny Islands. Depth profiles of Fe and δ^{56}Fe show the influence of input of Fe to surface waters from an island source for stations downstream of the Balleny Islands (Stations 13, 14), while waters at the station upstream (Station 15) exhibit a different profile shape. The grey bar represents the winter mixed layer as identified by the temperature minimum. (b) ACE stations near the Balleny Islands (Stations 13 - 15) plotted on a map of chlorophyll-*a*, based on satellite observations during the time of sampling (February 2017; NASA-OBPG, 2018).

δ^{56}Fe signatures (~−0.5‰). Below the WML, Fe concentrations slowly increase with depth, consistent with the trend described above for open ocean stations (Section 4.1). However, Station 14 shows a change to positive δ^{56}Fe at 200 m, while Station 13 returns to ~0‰ at this depth. These elevated δ^{56}Fe values at depths of 200-250 m at Station 14 may relate to volcanic activity near the Balleny Islands (see Section 4.2.3), but their exact cause remains unknown.

4.2.3. Deep heavy isotope anomaly – hydrothermal influence?

Positive δ^{56}Fe anomalies that are not associated with a significant change in Fe concentrations are seen at Station 15 (+1.8‰, 1000 m, Fig. 7a) and Station 22 (+2.0‰, 800 m, Fig. 6c). While the observation of such heavy isotope signatures at depth is unusual and the value of +2‰ is observed in a single datum at Station 22, the δ^{56}Fe profile at Station 15 increases with depth in an oceanographically consistent manner, and the majority of the subsurface water column profiles at both stations are isotopically heavy (+0.4 to +2‰ below 500 m). Furthermore, both stations are located near possible hydrothermal sources, a seamount chain east of the Balleny Islands (Station 15), and the East Scotia Ridge and South Sandwich Arc (Station 22). The Balleny Islands were formed by volcanic activity associated with the Balleny hotspot, with seismic activity and satellite inference of ash eruptions as re-

cently as 2001 (Global Volcanism Program, 2001) suggesting local volcanic, and thus hydrothermal, activity. The Scotia Arc and the South Sandwich Arc both have active vents, but only the Scotia Arc vents have previously been studied for Fe isotopes (Klar et al., 2017; Lough et al., 2017). As such, it is conceivable that these elevated δ^{56}Fe signatures might be related to hydrothermal Fe input.

While we have no constraints on a potential δ^{56}Fe signature of hydrothermal Fe near the Balleny Islands, hydrothermal vents at the East Scotia Ridge have previously been documented to release isotopically light Fe into the water column, with δ^{56}Fe values varying from -1 to -0.3‰ as the hydrothermal plumes undergo limited dilution and dissolved Fe concentrations decrease (Klar et al., 2017). In contrast, our postulated hydrothermal δ^{56}Fe signal is isotopically heavy. However, the previously analyzed isotopically light non-buoyant Scotia Arc plumes are still relatively proximal to their source, as seen by their high dissolved Fe concentrations (7-15 nmol kg^{-1}; Klar et al., 2017). By contrast, our samples have dissolved Fe concentrations typical for SZ waters at these depths (~0.4 nM), suggesting transport and greater dilution of any potential hydrothermal Fe. Such processes have been shown to affect the δ^{56}Fe of distal Fe in some settings. For example, similarly-high δ^{56}Fe values at background Fe concentrations have been observed near the Brothers underwater volcano in the Tonga-Kermadec arc system, where the primary hydrothermal signature of ~0‰ appears to fractionate to $> +1.5$‰ with vertical distance in the hydrothermal plume (Ellwood et al., 2015). That study interpreted this as the effect of fractionation of the primary δ^{56}Fe due to precipitation/scavenging, but it is also consistent with more recent studies from the East Pacific Rise that show primary venting as isotopically light, but distal dissolved hydrothermal Fe persisting as isotopically heavy ligand-bound Fe (Fitzsimmons et al., 2017). It is important to note that in both cases, vertically or laterally distal high δ^{56}Fe values in the water column do not reflect the primary hydrothermal vent δ^{56}Fe source signature, but are instead the result of fractionation associated with precipitation or the loss of specific phases of Fe as hydrothermal Fe is advected away from the vent. While such processes related to hydrothermal activity are not yet fully understood, they could explain the heavy Fe isotope anomalies observed in our dataset near the East Scotia Arc and near the Balleny Islands, and potentially affect the deep water δ^{56}Fe distribution in parts of the Southern Ocean.

4.3. AAIW and sources of Fe to low-latitude water masses

A major feature of the Southern Ocean is the formation of SAMW and AAIW by deep winter convection and subsequent subduction, specifically in the subantarctic South Pacific (e.g. Sallée et al., 2010). These upper-ocean water masses play an important role in supplying nutrients to the low-latitude surface ocean and control the global-scale distribution of macronutrients and many bioactive trace metals (e.g. Sarmiento et al., 2004; Vance et al., 2017). Furthermore, for some elements like Cd or Si, these water masses carry characteristic heavy isotope signatures that reflect their surface-ocean origin, resulting from biological uptake and mixing processes in their formation regions in the surface Southern Ocean (e.g. Fripiat et al., 2011; Abouchami et al., 2014). Abadie et al. (2017) have associated Atlantic AAIW with a δ^{56}Fe minimum (-0.17 to -0.27‰) that they attributed to regeneration within AAIW en route from the Southern Ocean, while Fitzsimmons et al. (2016) have suggested that a δ^{56}Fe minimum (-0.2‰) in AAIW in the southeast Pacific represents either a preformed signature or is the result of external Fe inputs after formation. AAIW is formed mainly in the southeast Pacific, close to the Drake Passage, by subduction of AASW during deep winter convection (Sallée et al., 2010). Our high-resolution dataset includes two stations (Stas. 19 & 20) near the main formation region of AAIW, making them ideal for studying the δ^{56}Fe signature of surface and near-surface waters that represent the source of AAIW. Specifically, do processes close to AAIW source regions impart a characteristic δ^{56}Fe to AAIW?

The upper ocean (top ~100 m) at Station 19 exhibits low Fe and elevated δ^{56}Fe values, showing that Fe in AASW and the WML (~100 m) is strongly controlled by biological uptake and Fe-binding ligands (Section 4.1). North of the APF, at Station 20, low Fe concentrations and high δ^{56}Fe extend to greater depths, consistent with deeper mixing (~200 m). Assuming the deep WMLs north of the APF act as a precursor for the δ^{56}Fe signature found in AAIW, as they do for other trace metals (Sieber et al., 2019b, 2020), we can conclude that Southern Ocean surface processes must impart a slightly heavy Fe isotopic signature to AAIW (Fig. 2). However, AAIW in the South Atlantic and the southeast Pacific bears low δ^{56}Fe (Fitzsimmons et al., 2016; Abadie et al., 2017), and AAIW in the southwest Pacific does not show any characteristic δ^{56}Fe signature (Conway et al., 2018). Furthermore, Fe concentrations in AAIW in these regions are considerably higher (up to 0.6 nmol kg^{-1}) than in the WMLs in the formation region of AAIW. Therefore, the lack of any significant northward transport of the biological surface Fe isotope signal is likely the result of the relatively short residence time of iron within the water mass, the low preformed Fe inventory, and the influence of external Fe sources, scavenging and regeneration processes (Tagliabue et al., 2019).

Based on our analysis of the circumpolar systematics of Fe and δ^{56}Fe, however, we are able to infer a possible alternative source of the light Fe signal previously observed in southeastern Atlantic AAIW, on GEOTRACES sections GA10 and GIPY04 (Conway et al., 2016; Abadie et al., 2017). Firstly, we have shown that light Fe from sediment sources on the Antarctic Peninsula influences subsurface waters of the Weddell Gyre, but does not reach the main formation region of AAIW (Section 4.2.1). Secondly, in our dataset, regeneration is not associated with a light isotope excursion, likely due to fractionation associated with scavenging and complexation by organic ligands at shallow depths, and the fact that regeneration happens gradually over a large depth range. Furthermore, the δ^{56}Fe signal of sinking biological material would most likely reflect the overall signature of Fe supplied to the mixed layer, which is ~0‰ or isotopically heavy over most of the Southern Ocean (this work; Abadie et al., 2017). As such, the light Fe signal in AAIW observed in the Atlantic Sector is unlikely to be from regeneration.

Thus, the light signature in Atlantic AAIW must instead be acquired after the formation of this water mass. Potential Fe sources are hydrothermal venting in the South Atlantic and sediments on the continental shelf of the Antarctic Peninsula. Specifically, dissolved Fe concentration anomalies (0.75–1.75 nmol kg^{-1}; Fig. 8a) have been observed at 55°S 0°E on the GIPY05e section, the southern extension of GIPY04, at depths of 400–3000 m (Klunder et al., 2011; Schlitzer et al., 2018). Klunder et al. (2011) have associated the elevated Fe concentrations in deep waters along GIPY05e with hydrothermal venting in the Bouvet region, and the Fe maximum at shallower depths with a distal continental shelf source from the Antarctic Peninsula. While the hydrothermal inputs are likely too deep (>1500 m), addition of isotopically light Fe along the shelf of the Antarctic Peninsula (see Section 4.2.1) and its subsequent eastward transport would be a plausible source to explain the lightest δ^{56}Fe signatures (–0.7‰) seen within UCDW at 52°S 0°E on GIPY04 at depths of 450 m (Abadie et al., 2017). The influence of northward moving UCDW can be seen in the high subsurface phosphate concentrations (1000 – 1500 m; Fig. 8b) in waters north of the ACC, below AAIW (picked out by salinity minimum in Fig. 8b). Abadie et al. (2017) then showed that mixing of UCDW with other water masses was the source of light Fe to AAIW.

Overall, this leads us to suggest that waters of the ACC pick up isotopically light Fe as they impinge upon and flow along the outer shelf of the Antarctic Peninsula, enabling transport into Atlantic

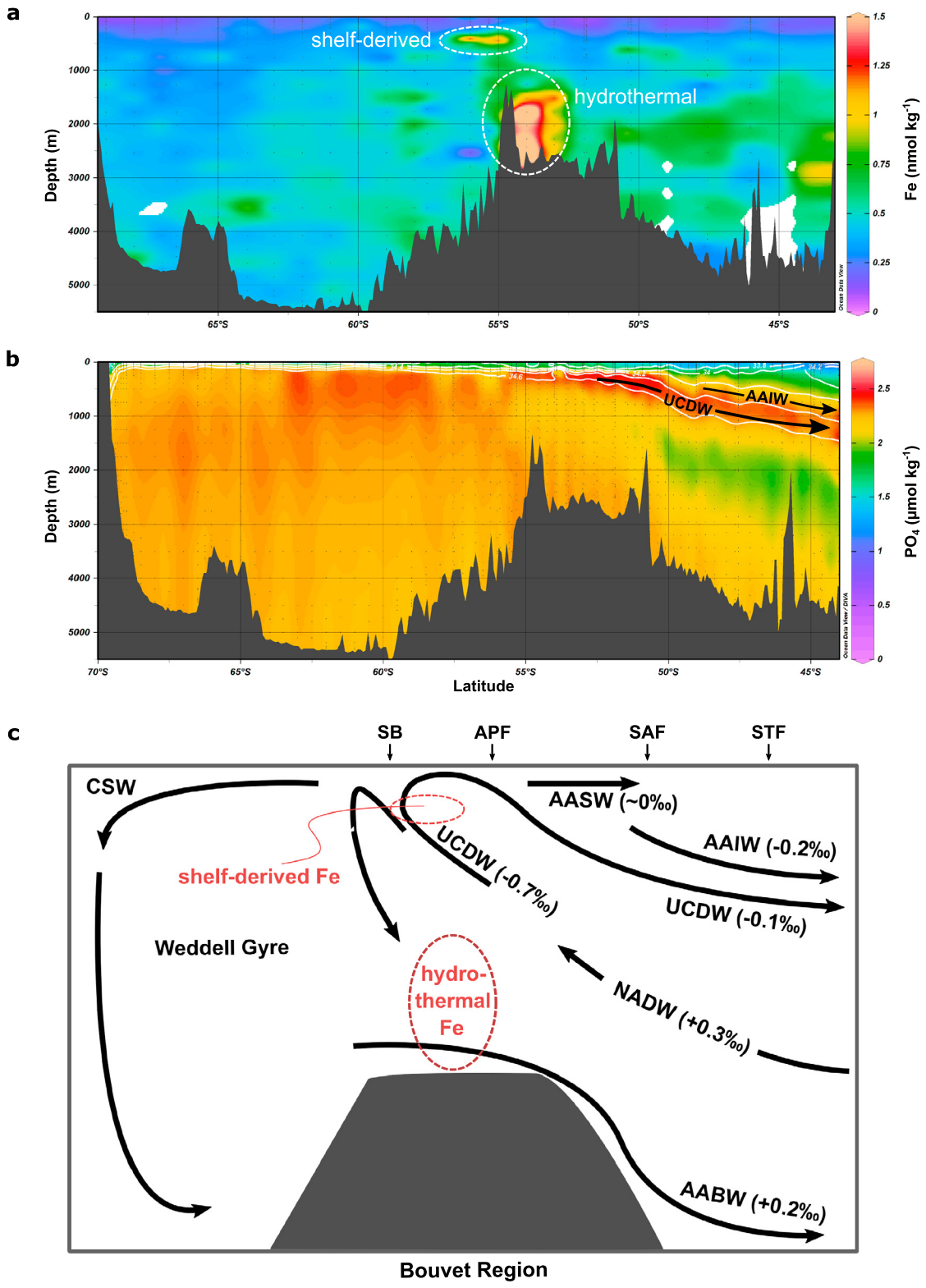

Fig. 8. Large scale Fe isotope cycling in the Southern Atlantic Ocean. (a) Section plot of dissolved Fe from GIPY04 (Schlitzer et al., 2018) showing elevated dissolved Fe due to hydrothermal vent input near the ridge in the Bouvet region and a shallower Fe maximum (400 – 700 m) derived from sedimentary inputs on the shelf of the Antarctic Peninsula (Klunder et al., 2011). (b) Section plot of salinity (contours), overlain on phosphate from GIPY04 (Schlitzer et al., 2018) showing elevated phosphate concentrations associated with UCDW. (c) Simplified circulation of the South Atlantic, adapted from Abadie et al. (2017). Hydrothermal Fe inputs in the Bouvet Region are likely too deep to affect UCDW. Instead, isotopically light Fe in UCDW might be derived from Fe inputs on the shelf of the Antarctic Peninsula. Mid-depth enhancement of eddy mixing over topography and north of the ACC (e.g. Watson et al., 2013) is the most likely pathway of light Fe into AAIW. Iron isotope signatures of the water masses are based on Abadie et al. (2017) and Conway et al. (2016).

UCDW. Upwelling of light Fe would explain the lack of high δ^{56}Fe in AASW along GIPY04 (Abadie et al., 2017), causing a shift from the isotope systematics described in Section 4.1. Vigorous eddy-driven mixing, both along and across isopycnals, within the ACC and at its northern flank (e.g. Watson et al., 2013) may drive mixing of UCDW and AAIW, thus imparting a slightly isotopically light δ^{56}Fe signature to AAIW. This influence on the δ^{56}Fe signature of the intermediate-depth South Atlantic can be seen at least as far as 40°S (Fig. 8c; Conway et al., 2016; Abadie et al., 2017; Schlitzer et al., 2018). Our hypothesis suggests that the AAIW signature ultimately reflects an external source signature rather than arising from internal cycling. External sources such as reductive sedimentary release may additionally influence AAIW δ^{56}Fe further north in the Atlantic (Conway et al., 2016), analogous to the southeast Pacific (Fitzsimmons et al., 2016). However, more δ^{56}Fe data in the Southern Ocean is needed to resolve this issue and fully understand the dominant processes controlling δ^{56}Fe in AAIW.

5. Conclusion

We have presented the first high-depth-resolution dissolved Fe and δ^{56}Fe data from all major Southern Ocean zones, using samples from the Antarctic Circumnavigation Expedition. We propose that the elevated δ^{56}Fe signals associated with very low Fe concentrations in surface waters are controlled by a series of surface processes (biological uptake, recycling, and binding of Fe to organic ligands) occurring above the ferricline. Due to the deep ferricline, there is a limited resupply of dissolved Fe from below, and subsurface δ^{56}Fe values are relatively homogenous down to 1000 m depth, with no obvious isotope signal associated with regeneration. This overall pattern is modified by the addition of dissolved Fe with characteristic δ^{56}Fe signatures at the local-to-regional scale in the vicinity of islands, the continental shelf or hydrothermal vents. Near the Balleny Islands, natural Fe fertilization occurs via input of isotopically light Fe to surface waters. With distance from the islands, the light isotope signal is preserved in the WML, but the surface signal transitions back to heavy values, driven by the surface δ^{56}Fe cycling regime observed elsewhere under Fe limitation. High δ^{56}Fe values at depth near the Balleny seamount chain and near the East Scotia Arc could be the result of distal hydrothermal influences, due to fractionation associated with precipitation or the loss of specific phases of Fe during transport of hydrothermal Fe from the vent. While the Antarctic margin provides sedimentary sources of isotopically light Fe to shelf waters, the long-distance transport of this Fe and its influence on surface waters are strongly dependent on regional circulation. As such, shelf currents along the Antarctic Peninsula transport light Fe into the Weddell Gyre but prevent its transport northwards, thus precluding any direct influence on the main formation region of AAIW in the subantarctic Pacific. Even though Southern Ocean surface processes must impart a heavy preformed δ^{56}Fe signature to AAIW, no characteristic source δ^{56}Fe signal is conserved as AAIW is exported to the lower latitudes. Instead, we suggest that light δ^{56}Fe signatures previously observed in Atlantic AAIW reflect interaction of the ACC with sedimentary Fe sources along the shelf of the Antarctic Peninsula. Shelf-derived isotopically light Fe is transported into Atlantic UCDW and subsequently mixed into AAIW within the ACC. In summary, our study highlights how the complex interaction of surface processes controls the δ^{56}Fe distribution across the upper Southern Ocean, and shows the importance of local Fe sources modifying this pattern and imparting characteristic isotope signatures.

CRediT authorship contribution statement

D.V., T.M.C., C.S.H. and M.J.E. planned the investigation. M.S., G.F.d.S., C.S.H. and M.J.E. contributed to sample collection during fieldwork. M.S. and T.M.C. carried out sample analysis. M.S., T.M.C., G.F.d.S. and D.V. interpreted the data. M.S. wrote the initial manuscript, and all authors contributed during the editing and reviewing of the manuscript.

Declaration of competing interest

The authors declare that they have no known competing financial interests or personal relationships that could have appeared to influence the work reported in this paper.

Acknowledgements

We thank the captain, crew and water sampling team aboard R/V Akademik Tryoshnikov on the Antarctic Circumnavigation Expedition, Corey Archer for assistance in the lab at ETH Zurich and Ethan Goddard for technical assistance at the University of South Florida. This study was supported by ETH Zurich, the University of South Florida, and Project 15 of the Antarctic Circumnavigation Expedition (funded by EPFL, Swiss Polar Institute and Ferring Pharmaceuticals). We thank Michael Staubwasser and an anonymous reviewer for their comments, which helped us strengthen this manuscript. Finally, we wish to thank the late David Walton, chief scientist for the expedition, for his support at sea.

Appendix A. Supplementary material

Supplementary material related to this article can be found online at https://doi.org/10.1016/j.epsl.2021.116967.

References

Abadie, C., Lacan, F., Radic, A., Pradoux, C., Poitrasson, F., 2017. Iron isotopes reveal distinct dissolved iron sources and pathways in the intermediate versus deep Southern Ocean. Proc. Natl. Acad. Sci. USA 114, 858–863. https://doi.org/10.1073/pnas.1603107114.

Abouchami, W., Galer, S.J.G., De Baar, H.J.W., Middag, R., Vance, D., Zhao, Y., Klunder, M., Mezger, K., Feldmann, H., Andreae, M.O., 2014. Biogeochemical cycling of cadmium isotopes in the Southern Ocean along the Zero Meridian. Geochim. Cosmochim. Acta 127, 348–367. https://doi.org/10.1016/j.gca.2013.10.022.

Ardelan, M.V., Holm-Hansen, O., Hewes, C.D., Reiss, C.S., Silva, N.S., Dulaiova, H., Steinnes, E., Sakshaug, E., 2010. Natural iron enrichment around the Antarctic Peninsula in the Southern Ocean. Biogeosciences 7, 11–25. https://doi.org/10.5194/bg-7-11-2010.

Ardyna, M., Lacour, L., Sergi, S., D'Ovidio, F., Sallée, J.-B.B., Rembauville, M., Blain, S., Tagliabue, A., Schlitzer, R., Jeandel, C., Arrigo, K.R., Claustre, H., 2019. Hydrothermal vents trigger massive phytoplankton blooms in the Southern Ocean. Nat. Commun. 10. https://doi.org/10.1038/s41467-019-09973-6.

Arrigo, K.R., van Dijken, G.L., Strong, A.L., 2015. Environmental controls of marine productivity hot spots around Antarctica. J. Geophys. Res., Oceans 120, 5545–5565. https://doi.org/10.1002/2015JC010888.

Beard, B.L., Johnson, C.M., Von Damm, K.L., Poulson, R.L., 2003. Iron isotope constraints on Fe cycling and mass balance in oxygenated Earth oceans. Geology 31, 629–632. https://doi.org/10.1130/0091-7613(2003)031<0629:iicofc>2.0.co;2.

Bowie, A.R., Maldonado, M.T., Frew, R.D., Croot, P.L., Achterberg, E.P., Mantoura, R.F.C., Worsfold, P.J., Law, C.S., Boyd, P.W., 2001. The fate of added iron during a mesoscale fertilisation experiment in the Southern Ocean. Deep-Sea Res., Part 2, Top. Stud. Oceanogr. 48, 2703–2743. https://doi.org/10.1016/S0967-0645(01)00015-7.

Boyd, P.W., Ellwood, M.J., 2010. The biogeochemical cycle of iron in the ocean. Nat. Geosci. 3, 675–682. https://doi.org/10.1038/ngeo964.

Conway, T.M., John, S.G., Lacan, F., 2016. Intercomparison of dissolved iron isotope profiles from reoccupation of three GEOTRACES stations in the Atlantic Ocean. Mar. Chem. 183, 50–61. https://doi.org/10.1016/J.MARCHEM.2016.04.007.

Conway, T.M., Rosenberg, A.D., Adkins, J.F., John, S.G., 2013. A new method for precise determination of iron, zinc and cadmium stable isotope ratios in seawater by double-spike mass spectrometry. Anal. Chim. Acta 793, 44–52. https://doi.org/10.1016/j.aca.2013.07.025.

Conway, T.M., John, S.G., 2014. Quantification of dissolved iron sources to the North Atlantic Ocean. Nature 511, 212–215. https://doi.org/10.1038/nature13482.

Conway, T.M., Sieber, M., Ellwood, M.E., Takano, S., Sohrin, Y., Vance, D., 2018. The competing influence of local cycling, regional sources and Southern Ocean processes in influencing Fe isotope cycling at lower latitudes in the oceans. In: Ocean Sciences Meeting 2018, Portland.

de Jong, J., Schoemann, V., Lannuzel, D., Croot, P., De Baar, H., Tison, J., de Baar, H., Tison, J., 2012. Natural iron fertilization of the Atlantic sector of the Southern Ocean by continental shelf sources of the Antarctic Peninsula. J. Geophys. Res. 117. https://doi.org/10.1029/2011JG001679.

Dideriksen, K., Baker, J.A., Stipp, S.L.S., 2008. Equilibrium Fe isotope fractionation between inorganic aqueous Fe(III) and the siderophore complex, Fe(III)-desferrioxamine B. Earth Planet. Sci. Lett. 269, 280–290. https://doi.org/10.1016/j.epsl.2008.02.022.

Ellwood, M.J., Strzepek, R.F., Strutton, P.G., Trull, T.W., Fourquez, M., Boyd, P.W., 2020. Distinct iron cycling in a Southern Ocean eddy. Nat. Commun. 11, 825. https://doi.org/10.1038/s41467-020-14464-0.

Ellwood, M.J., Hutchins, D.A., Lohan, M.C., Milne, A., Nasemann, P., Nodder, S.D., Sander, S.G., Strzepek, R., Wilhelm, S.W., Boyd, P.W., 2015. Iron stable isotopes track pelagic iron cycling during a subtropical phytoplankton bloom. Proc. Natl. Acad. Sci. USA 112 E15-20, https://doi.org/10.1073/pnas.1421576112.

Fitzsimmons, J.N., Carrasco, G.G., Wu, J., Roshan, S., Hatta, M., Measures, C.I., Conway, T.M., John, S.G., Boyle, E.A., 2015. Partitioning of dissolved iron and iron isotopes into soluble and colloidal phases along the GA03 GEOTRACES, North Atlantic Transect. Deep-Sea Res., Part 2, Top. Stud. Oceanogr. 116, 130–151. https://doi.org/10.1016/j.dsr2.2014.11.014.

Fitzsimmons, J.N., Conway, T.M., Lee, J.-M., Kayser, R., Thyng, K.M., John, S.G., Boyle, E.A., 2016. Dissolved iron and iron isotopes in the southeastern Pacific Ocean. Glob. Biogeochem. Cycles 30, 1372–1395. https://doi.org/10.1002/2015GB005357.

Fitzsimmons, J.N., John, S.G., Marsay, C.M., Hoffman, C.L., Nicholas, S.L., Toner, B.M., German, C.R., Sherrell, R.M., 2017. Iron persistence in a distal hydrothermal plume supported by dissolved-particulate exchange. Nat. Geosci. 10, 195–201. https://doi.org/10.1038/ngeo2900.

Fripiat, F., Cavagna, A.-J., Dehairs, F., Speich, S., André, L., Cardinal, D., 2011. Silicon pool dynamics and biogenic silica export in the Southern Ocean inferred from Si-isotopes. Ocean Sci. 7, 533–547. https://doi.org/10.5194/os-7-533-2011.

Gerringa, L.J.A., Laan, P., van Dijken, G.L., van Haren, H., De Baar, H.J.W., Arrigo, K.R., Alderkamp, A.-C., 2015. Sources of iron in the Ross Sea Polynya in early summer. Mar. Chem. 177, 447–459. https://doi.org/10.1016/J.MARCHEM.2015.06.002.

Gruber, N., Landschützer, P., Lovenduski, N.S., 2019. The variable Southern Ocean carbon sink. Annu. Rev. Mar. Sci. 11, 159–186. https://doi.org/10.1146/annurev-marine-121916-063407.

Hamilton, D.S., Scanza, R.A., Feng, Y., Guinness, J., Kok, J.F., Li, L., Liu, X., Rathod, S.D., Wan, J.S., Wu, M., Mahowald, N.M., 2019. Improved methodologies for Earth system modelling of atmospheric soluble iron and observation comparisons using the Mechanism of Intermediate complexity for Modelling Iron (MIMI v1.0). Geosci. Model Dev. 12, 3835–3862. https://doi.org/10.5194/gmd-12-3835-2019.

Hatta, M., Measures, C.I., Selph, K.E., Zhou, M., Hiscock, W.T., 2013. Iron fluxes from the shelf regions near the South Shetland Islands in the Drake Passage during the austral-winter 2006. Deep-Sea Res., Part 2, Top. Stud. Oceanogr. 90, 89–101. https://doi.org/10.1016/J.DSR2.2012.11.003.

Henkel, S., Kasten, S., Hartmann, J.F., Silva-Busso, A., Staubwasser, M., 2018. Iron cycling and stable Fe isotope fractionation in Antarctic shelf sediments, King George Island. Geochim. Cosmochim. Acta 237, 320–338. https://doi.org/10.1016/J.GCA.2018.06.042.

Homoky, W.B., John, S.G., Conway, T.M., Mills, R.A., 2013. Distinct iron isotopic signatures and supply from marine sediment dissolution. Nat. Commun. 4, 2143. https://doi.org/10.1038/ncomms3143.

Ilina, S.M., Poitrasson, F., Lapitskiy, S.A., Alekhin, Y.V., Viers, J., Pokrovsky, O.S., 2013. Extreme iron isotope fractionation between colloids and particles of boreal and temperate organic-rich waters. Geochim. Cosmochim. Acta 101, 96–111. https://doi.org/10.1016/j.gca.2012.10.023.

Janssen, D.J., Sieber, M., Ellwood, M.J., Conway, T.M., Barrett, P.M., Chen, X., de Souza, G.F., Hassler, C.S., Jaccard, S.L., 2020. Trace metal and nutrient dynamics across broad biogeochemical gradients in the Indian and Pacific sectors of the Southern Ocean. Mar. Chem. 221, 103773. https://doi.org/10.1016/j.marchem.2020.103773.

Jiang, M., Measures, C.I., Barbeau, K.A., Charette, M.A., Gille, S.T., Hatta, M., Kahru, M., Mitchell, B.G., Naveira Garabato, A.C., Reiss, C., Selph, K., Zhou, M., 2019. Fe sources and transport from the Antarctic Peninsula shelf to the southern Scotia Sea. Deep-Sea Res., Part 1, Oceanogr. Res. Pap. 103060. https://doi.org/10.1016/J.DSR.2019.06.006.

Klar, J.K., James, R.H., Gibbs, D., Lough, A., Parkinson, I., Milton, J.A., Hawkes, J.A., Connelly, D.P., 2017. Isotopic signature of dissolved iron delivered to the Southern Ocean from hydrothermal vents in the East Scotia Sea. Geology 45, 351–354. https://doi.org/10.1130/G38432.1.

Klunder, M.B., Laan, P., De Baar, H.J.W., Middag, R., Neven, I., Van Ooijen, J., 2014. Dissolved Fe across the Weddell Sea and Drake Passage: impact of DFe on nutrient uptake. Biogeosciences 11, 651–669. https://doi.org/10.5194/bg-11-651-2014.

Klunder, M.B., Laan, P., Middag, R., De Baar, H.J.W., Van Ooijen, J.C., 2011. Dissolved iron in the Southern Ocean (Atlantic sector). Deep-Sea Res., Part 2, Top. Stud. Oceanogr. 58, 2678–2694. https://doi.org/10.1016/j.dsr2.2010.10.042.

Lannuzel, D., Vancoppenolle, M., Van Der Merwe, P., De Jong, J., Meiners, K.M., Grotti, M., Nishioka, J., Schoemann, V., 2016. Iron in sea ice: review & new insights. Elementa 4, 000130. https://doi.org/10.12952/journal.elementa.000130.

Lough, A.J.M., Klar, J.K., Homoky, W.B., Comer-Warner, S.A., Milton, J.A., Connelly, D.P., James, R.H., Mills, R.A., 2017. Opposing authigenic controls on the isotopic signature of dissolved iron in hydrothermal plumes. Geochim. Cosmochim. Acta 202, 1–20. https://doi.org/10.1016/j.gca.2016.12.022.

Measures, C.I., Brown, M.T., Selph, K.E., Apprill, A., Zhou, M., Hatta, M., Hiscock, W.T., 2013. The influence of shelf processes in delivering dissolved iron to the HNLC waters of the Drake Passage, Antarctica. Deep-Sea Res., Part 2, Top. Stud. Oceanogr. 90, 77–88. https://doi.org/10.1016/J.DSR2.2012.11.004.

Moore, C.M., Mills, M.M., Arrigo, K.R., Berman-Frank, I., Bopp, L., Boyd, P.W., Galbraith, E.D., Geider, R.J., Guieu, C., Jaccard, S.L., Jickells, T.D., La Roche, J., Lenton, T.M., Mahowald, N.M., Marañón, E., Marinov, I., Moore, J.K., Nakatsuka, T., Oschlies, A., Saito, M.A., Thingstad, T.F., Tsuda, A., Ulloa, O., 2013. Processes and patterns of oceanic nutrient limitation. Nat. Geosci. 6, 701–710. https://doi.org/10.1038/ngeo1765.

Moore, J.K.K., Doney, S.C., Glover, D.M., Fung, I.Y., 2002. Iron cycling and nutrient-limitation patterns in surface waters of the World Ocean. Deep-Sea Res., Part 2, Top. Stud. Oceanogr. 49, 463–507. https://doi.org/10.1016/S0967-0645(01)00109-6.

Morel, F.M.M., Milligan, A.J., Saito, M.A., 2014. Marine bioinorganic chemistry: the role of trace metals in the oceanic cycles of major nutrients. In: Treatise on Geochemistry. Elsevier, pp. 123–150.

Morgan, J.L.L., Wasylenki, L.E., Nuester, J., Anbar, A.D., 2010. Fe isotope fractionation during equilibration of Fe-organic complexes. Environ. Sci. Technol. 44, 6095–6101. https://doi.org/10.1021/es100906z.

Orsi, A.H., Whitworth, T., Nowlin, W.D., 1995. On the meridional extent and fronts of the Antarctic Circumpolar Current. Deep-Sea Res., Part 1, Oceanogr. Res. Pap. 42, 641–673. https://doi.org/10.1016/0967-0637(95)00021-W.

Planquette, H., Sanders, R.R., Statham, P.J., Morris, P.J., Fones, G.R., 2011. Fluxes of particulate iron from the upper ocean around the Crozet Islands: a naturally iron-fertilized environment in the Southern Ocean. Glob. Biogeochem. Cycles 25 n/a-n/a, https://doi.org/10.1029/2010GB003789.

Radic, A., Lacan, F., Murray, J.W., 2011. Iron isotopes in the seawater of the equatorial Pacific Ocean: new constraints for the oceanic iron cycle. Earth Planet. Sci. Lett. 306, 1–10. https://doi.org/10.1016/j.epsl.2011.03.015.

Rafter, P.A., Sigman, D.M., Mackey, K.R.M., 2017. Recycled iron fuels new production in the eastern equatorial Pacific Ocean. Nat. Commun. 8, 1100. https://doi.org/10.1038/s41467-017-01219-7.

Resing, J.A., Sedwick, P.N., German, C.R., Jenkins, W.J., Moffett, J.W., Sohst, B.M., Tagliabue, A., 2015. Basin-scale transport of hydrothermal dissolved metals across the South Pacific Ocean. Nature 523, 200–203. https://doi.org/10.1038/nature14577.

Sallée, J.-B., Speer, K., Rintoul, S., Wijffels, S., 2010. Southern Ocean thermocline ventilation. J. Phys. Oceanogr. 40, 509–529. https://doi.org/10.1175/2009JPO4291.1.

Sarmiento, J.L., Gruber, N., Brzezinski, M.A., Dunne, J.P., 2004. High-latitude controls of thermocline nutrients and low latitude biological productivity. Nature 427, 56–60. https://doi.org/10.1038/nature10605.

Sarmiento, J.L., Simeon, J., Gnanadesikan, A., Gruber, N., Key, R.M., Schlitzer, R., 2007. Deep ocean biogeochemistry of silicic acid and nitrate. Glob. Biogeochem. Cycles 21, 1–16. https://doi.org/10.1029/2006GB002720.

Schlitzer, R., Anderson, R.F., Dodas, E.M., Lohan, M., Geibert, W., Tagliabue, A., Bowie, A., Jeandel, C., Maldonado, M.T., Landing, W.M., Cockwell, D., Abadie, C., Abouchami, W., Achterberg, E.P., Agather, A., Aguliar-Islas, A., van Aken, H.M., Andersen, M., Archer, C., Auro, M., de Baar, H.J., Baars, O., Baker, A.R., Bakker, K., Basak, C., Baskaran, M., Bates, N.R., Bauch, D., van Beek, P., Behrens, M.K., Black, E., Bluhm, K., Bopp, L., Bouman, H., Bowman, K., Bown, J., Boyd, P., Boye, M., Boyle, E.A., Branellec, P., Bridgestock, L., Brissebrat, G., Browning, T., Bruland, K.W., Brumsack, H.-J., Brzezinski, M., Buck, C.S., Buck, K.N., Buesseler, K., Bull, A., Butler, E., Cai, P., Mor, P.C., Cardinal, D., Carlson, C., Carrasco, G., Casacuberta, N., Casciotti, K.L., Castrillejo, M., Chamizo, E., Chance, R., Charette, M.A., Chaves, J.E., Cheng, H., Chever, F., Christl, M., Church, T.M., Closset, I., Colman, A., Conway, T.M., Cossa, D., Croot, P., Cullen, J.T., Cutter, G.A., Daniels, C., Dehairs, F., Deng, F., Dieu, H.T., Duggan, B., Dulaquais, G., Dumousseaud, C., Echegoyen-Sanz, Y., Edwards, R.L., Ellwood, M., Fahrbach, E., Fitzsimmons, J.N., Russell Flegal, A., Fleisher, M.Q., van de Flierdt, T., Frank, M., Friedrich, J., Fripiat, F., Fröllje, H., Galer, S.J.G., Gamo, T., Ganeshram, R.S., Garcia-Orellana, J., Garcia-Solsona, E., Gault-Ringold, M., George, E., Gerringa, L.J.A., Gilbert, M., Godoy, J.M., Goldstein, S.L., Gonzalez, S.R., Grissom, K., Hammerschmidt, C., Hartman, A., Hassler, C.S., Hathorne, E.C., Hatta, M., Hawco, N., Hayes, C.T., Heimbürger, L.-E., Helgoe, J., Heller, M., Henderson, G.M., Henderson, P.B., van Heuven, S., Ho, P., Horner, T.J., Hsieh, Y.-T., Huang, K.-F., Humphreys, M.P., Isshiki, K., Jacquot, J.E., Janssen, D.J., Jenkins, W.J., John, S., Jones, E.M., Jones, J.L., Kadko, D.C., Kayser, R., Kenna, T.C., Khondoker, R., Kim, T., Kipp, L., Klar, J.K., Klunder, M., Kretschmer, S., Kumamoto, Y., Laan, P., Labatut, M., Lacan, F., Lam, P.J., Lambelet, M., Lamborg, C.H., Le Moigne, F.A.C., Le Roy, E., Lechtenfeld, O.J., Lee, J.-M., Lherminier, P., Little, S., López-Lora, M., Lu, Y., Masque, P., Mawji, E., Mcclain, C.R., Measures, C., Mehic, S., Barraqueta, J.-L.M., van der Merwe, P., Middag, R., Mieruch, S., Milne, A., Minami, T., Moffett, J.W., Moncoiffe, G., Moore, W.S., Morris, P.J., Morton, P.L., Nakaguchi, Y., Nakayama, N., Niedermiller, J., Nishioka, J., Nishiuchi, A., Noble, A., Obata, H., Ober, S., Ohnemus, D.C., van Ooijen, J., O'Sullivan, J., Owens, S., Pahnke, K., Paul, M., Pavia, F., Pena, L.D., Peters, B., Planchon, F., Planquette, H., Pradoux,

C., Puigcorbé, V., Quay, P., Queroue, F., Radic, A., Rauschenberg, S., Rehkämper, M., Rember, R., Remenyi, T., Resing, J.A., Rickli, J., Rigaud, S., Rijkenberg, M.J.A., Rintoul, S., Robinson, L.F., Roca-Martí, M., Rodellas, V., Roeske, T., Rolison, J.M., Rosenberg, M., Roshan, S., Rutgers van der Loeff, M.M., Ryabenko, E., Saito, M.A., Salt, L.A., Sanial, V., Sarthou, G., Schallenberg, C., Schauer, U., Scher, H., Schlosser, C., Schnetger, B., Scott, P., Sedwick, P.N., Semiletov, I., Shelley, R., Sherrell, R.M., Shiller, A.M., Sigman, D.M., Singh, S.K., Slagter, H.A., Slater, E., Smethie, W.M., Snaith, H., Sohrin, Y., Sohst, B., Sonke, J.E., Speich, S., Steinfeldt, R., Stewart, G., Stichel, T., Stirling, C.H., Stutsman, J., Swarr, G.J., Swift, J.H., Thomas, A., Thorne, K., Till, C.P., Till, R., Townsend, A.T., Townsend, E., Tuerena, R., Twining, B.S., Vance, D., Velazquez, S., Venchiarutti, C., Villa-Alfageme, M., Vivancos, S.M., Voelker, A.H.L., Wake, B., Warner, M.J., Watson, R., van Weerlee, E., Alexandra Weigand, M., Weinstein, Y., Weiss, D., Wisotzki, A., Woodward, E.M.S., Wu, J., Wu, Y., Wuttig, K., Wyatt, N., Xiang, Y., Xie, R.C., Xue, Z., Yoshikawa, H., Zhang, J., Zhang, P., Zhao, Y., Zheng, L., Zheng, X.-Y., Zieringer, M., Zimmer, L.A., Ziveri, P., Zunino, P., Zurbrick, C., 2018. The GEOTRACES Intermediate Data Product 2017. Chem. Geol. 493, 210–223. https://doi.org/10.1016/J.CHEMGEO.2018.05.040.

Severmann, S., Johnson, C.M., Beard, B.L., German, C.R., Edmonds, H.N., Chiba, H., Green, D.R.H., 2004. The effect of plume processes on the Fe isotope composition of hydrothermally derived Fe in the deep ocean as inferred from the Rainbow vent site, Mid-Atlantic Ridge, 36 degrees 14' N. Earth Planet. Sci. Lett. 225, 63–76.

Sherrell, R.M., Annett, A.L., Fitzsimmons, J.N., Roccanova, V.J., Meredith, M.P., 2018. A 'shallow bathtub ring' of local sedimentary iron input maintains the Palmer Deep biological hotspot on the West Antarctic Peninsula shelf. Philos. Trans. R. Soc. A, Math. Phys. Eng. Sci. 376, 20170171. https://doi.org/10.1098/rsta.2017.0171.

Sieber, M., Conway, T.M., de Souza, G.F., Obata, H., Takano, S., Sohrin, Y., Vance, D., 2019a. Physical and biogeochemical controls on the distribution of dissolved cadmium and its isotopes in the Southwest Pacific Ocean. Chem. Geol. 511, 494–509. https://doi.org/10.1016/j.chemgeo.2018.07.021.

Sieber, M., Conway, T.M., de Souza, G.F., Hassler, C.S., Ellwood, M.J., Vance, D., 2019b. High-resolution Cd isotope systematics in multiple zones of the Southern Ocean from the Antarctic Circumnavigation Expedition. Earth Planet. Sci. Lett. 527, 115799. https://doi.org/10.1016/J.EPSL.2019.115799.

Sieber, M., Conway, T.M., de Souza, G.F., Hassler, C.S., Ellwood, M.J., Vance, D., 2020. Cycling of zinc and its isotopes across multiple zones of the Southern Ocean: insights from the Antarctic Circumnavigation Expedition. Geochim. Cosmochim. Acta 268, 310–324. https://doi.org/10.1016/j.gca.2019.09.039.

Siebert, C., Nägler, T.F., Kramers, J.D., 2001. Determination of molybdenum isotope fractionation by double-spike multicollector inductively coupled plasma mass spectrometry. Geochem. Geophys. Geosyst. 2. https://doi.org/10.1029/2000GC000124.

Tagliabue, A., Sallée, J.-B., Bowie, A.R., Lévy, M., Swart, S., Boyd, P.W., 2014. Surface-water iron supplies in the Southern Ocean sustained by deep winter mixing. Nat. Geosci. 7, 314–320. https://doi.org/10.1038/ngeo2101.

Tagliabue, A., Bowie, A.R., DeVries, T., Ellwood, M.J., Landing, W.M., Milne, A., Ohnemus, D.C., Twining, B.S., Boyd, P.W., 2019. The interplay between regeneration and scavenging fluxes drives ocean iron cycling. Nat. Commun. 10. https://doi.org/10.1038/s41467-019-12775-5.

Talley, L.D., Pickard, G.L., Emery, W.J., Swift, J.H., 2011. Descriptive Physical Oceanography: An Introduction. Academic Press.

Vance, D., Little, S.H., de Souza, G.F., Khatiwala, S., Lohan, M.C., Middag, R., 2017. Silicon and zinc biogeochemical cycles coupled through the Southern Ocean. Nat. Geosci. 10, 202. https://doi.org/10.1038/ngeo2890.

Watson, A.J., Ledwell, J.R., Messias, M.J., King, B.A., Mackay, N., Meredith, M.P., Mills, B., Naveira Garabato, A.C., 2013. Rapid cross-density ocean mixing at mid-depths in the Drake Passage measured by tracer release. Nature 501, 408–411. https://doi.org/10.1038/nature12432.